Anti-amyloid therapy protects against retinal pigmented epithelium damage and vision loss in a model of age-related macular degeneration

Jin-Dong Ding[a], Lincoln V. Johnson[b], Rolf Herrmann[a], Sina Farsiu[a], Stephanie G. Smith[a], Marybeth Groelle[a], Brian E. Mace[c], Patrick Sullivan[c], Jeffrey A. Jamison[d], Una Kelly[a], Ons Harrabi[e], Sangeetha Subbarao Bollini[e], Jeanette Dilley[e], Dione Kobayashi[e], Bing Kuang[f], Wenlin Li[f], Jaume Pons[e], John C. Lin[e,1], and Catherine Bowes Rickman[a,g,1]

[a]Department of Ophthalmology, Duke Eye Center, Duke University, Durham, NC 27710; [b]Center for the Study of Macular Degeneration, Neuroscience Research Institute, University of California, Santa Barbara, CA 93106; [c]Division of Geriatrics, Department of Medicine, Durham Veterans Affairs Hospitals Medical Center, Duke University, Durham, NC 27705; [d]Ophthy-DS, Inc., MPI Research, Inc., Mattawan, MI 49071; [e]Rinat, Pfizer Inc., South San Francisco, CA 94080; [f]Worldwide Research and Development, Pfizer Inc., La Jolla, CA 92121; and [g]Department of Cell Biology, Duke University, Durham, NC 27710

Edited by Alan Bird, University of London, London, United Kingdom, and accepted by the Editorial Board May 24, 2011 (received for review January 17, 2011)

Age-related macular degeneration (AMD) is a leading cause of visual dysfunction worldwide. Amyloid β (Aβ) peptides, Aβ1–40 (Aβ40) and Aβ1–42 (Aβ42), have been implicated previously in the AMD disease process. Consistent with a pathogenic role for Aβ, we show here that a mouse model of AMD that invokes multiple factors that are known to modify AMD risk (aged human *apolipoprotein E 4* targeted replacement mice on a high-fat, cholesterol-enriched diet) presents with Aβ-containing deposits basal to the retinal pigmented epithelium (RPE), histopathologic changes in the RPE, and a deficit in scotopic electroretinographic response, which is reflective of impaired visual function. Strikingly, these electroretinographic deficits are abrogated in a dose-dependent manner by systemic administration of an antibody targeting the C termini of Aβ40 and Aβ42. Concomitant reduction in the levels of Aβ and activated complement components in sub-RPE deposits and structural preservation of the RPE are associated with anti-Aβ40/42 antibody immunotherapy and visual protection. These observations are consistent with the reduction in amyloid plaques and improvement of cognitive function in mouse models of Alzheimer's disease treated with anti-Aβ antibodies. They also implicate Aβ in the pathogenesis of AMD and identify Aβ as a viable therapeutic target for its treatment.

Age-related macular degeneration (AMD) affects about 30% of Americans over 70 y of age (1–3) and is the leading cause of irreversible blindness in the Western world (4). It is a progressive retinal degenerative disease influenced by both environmental and genetic factors. Although the presence of a few small hard drusen is a normal, nonvision-impairing part of aging, the deposition of large diffuse drusen in the macula adversely impacts vision and is indicative of early AMD. As AMD progresses to late-stage disease, it is categorized as either dry [geographic atrophy with photoreceptor loss and extensive atrophy of the retinal pigmented epithelium (RPE)] or wet [exudative with subsequent choroidal neovascularization (CNV)] (5). Currently, there are no effective treatments for early AMD, and treatments for late-stage disease are limited to photodynamic therapy, macular translocation, and antivascular endothelial growth factor drugs (6–9).

The strongest known risk factors are advanced age and cigarette smoking, with additional risk conferred by body mass index and diets high in fat (1, 10–14). The last decade has also yielded strong evidence that genotype, especially for genes involved in inflammation and the innate immune system, influences AMD risk and progression. Genes implicated as risk factors include complement factor H (*CFH*) (15–18), complement factor B (19), complement C3 (20), apolipoprotein E (*APOE*) (21–25), toll-like receptor 4 (26), *LOC387715/ARMS2* (27, 28), *HTRA1* (29, 30), *ABCA4* (31), and fibulin 5 (32). Additional support for a role for chronic local inflammation in AMD comes from the discovery that protein components of drusen include activated components of the complement system (e.g., C3b and C5b-9), molecules involved in the acute-phase response to inflammation (e.g., amyloid P component), and proteins that modulate the immune response [e.g., CFH, vitronectin, clusterin/apolipoprotein J, apolipoprotein E (apoE), and amyloid β (Aβ)] (33–36).

Abnormal extracellular deposition of proteins may contribute to AMD pathogenesis and progression, which is the case in Alzheimer's disease and atherosclerosis. It is noteworthy that their respective pathophysiological deposits contain many shared constituents such as apoE, complement, and Aβ peptides. For instance, in human AMD, Aβ peptide deposition is associated with drusen, where it accumulates and colocalizes with activated complement components (37–39). Luibl et al. (40) showed the presence of potentially toxic amyloid oligomers in drusen, sub-RPE basal deposits, and RPE of human donor eyes using an antibody that specifically recognizes the oligomeric form of Aβ. These Aβ oligomers were not detected in control age-matched donor eyes without drusen. Isas et al. (41) also detected soluble as well as mature Aβ fibrils in drusen. Collectively, these findings implicate Aβ in the pathogenesis of AMD. In addition, we detected Aβ peptide in sub-RPE basal deposits and neovascular lesions in a murine model of AMD (42, 43). In this model, aged human *APOE4*-targeted replacement mice (*APOE4* mice) fed a high-fat, cholesterol-enriched (HFC) diet (*APOE4*-HFC mice) exhibit morphologic hallmarks observed in both dry and wet AMD. These hallmarks include thick diffuse sub-RPE deposits, lipid- and protein-containing focal drusen-like deposits, thickening of Bruch's membrane, patchy regions of RPE atrophy opposed to areas of photoreceptor degeneration, and CNV (43).

We hypothesized that, in the *APOE4*-HFC mouse model of AMD, Aβ accumulation provokes damage at the level of the RPE/choroid and previously showed that systemic administration of anti-Aβ40–specific antibodies can partially attenuate the decline in visual function exhibited in this model (42). Herein, we show that anti-Aβ immunotherapy simultaneously targeting both

Author contributions: J.-D.D., L.V.J., J.C.L., and C.B.R. designed research; J.-D.D., R.H., S.G.S., M.G., B.E.M., J.A.J., U.K., O.H., S.S.B., J.D., D.K., B.K., W.L., and J.P. performed research; S.F., P.S., and J.C.L. contributed new reagents/analytic tools; J.-D.D., L.V.J., R.H., S.F., S.G.S., J.A.J., U.K., B.K., J.C.L., and C.B.R. analyzed data; and C.B.R. wrote the paper.

Conflict of interest statement: O.H., S.S.B., J.D., D.K., B.K., W.L., J.P., and J.C.L. are full-time employees of Pfizer Inc., and Pfizer Inc. owns the intellectual properties of the antibodies described herein. L.V.J. and C.B.R. have received research funding from Pfizer Inc.

This article is a PNAS Direct Submission.

Freely available online through the PNAS open access option.

[1]To whom correspondence may be addressed. E-mail: john.lin@pfizer.com or bowes007@duke.edu.

See Author Summary on page 11307.

This article contains supporting information online at www.pnas.org/lookup/suppl/doi:10.1073/pnas.1100901108/-/DCSupplemental.

Aβ40 and Aβ42 blocks histopathologic changes and completely protects visual function in *APOE4*-HFC mice. This finding represents proof of principle evidence that targeting Aβ through systemic administration of anti-Aβ antibodies may be a promising therapeutic strategy for human AMD.

Results

Aβ Antibodies. Aβ-specific antibodies were generated by immunization with peptides containing the C-terminal amino acid sequence of Aβ40 or Aβ42 and screened for binding activity against Aβ40 and Aβ42. As a result, monoclonal antibodies specific for Aβ40 and Aβ42 and bispecific for Aβ40/42 were identified (Fig. S1 *A* and *B*). Epitope mapping for the Aβ40/42-bispecific antibody using a series of overlapping peptides covering the C-terminal one-half of Aβ (Fig. S1*C*) showed amino acids 25–34 to be minimally required for binding. In separate experiments, we found that extension of the minimal Aβ epitope to include residue 40 also enhances the binding affinity. Because the epitope of the Aβ40/42-bispecific antibody lies partly within the transmembrane domain of human amyloid precursor protein (hAPP) (Fig. S1*D*), this antibody was not expected to bind full-length, uncleaved hAPP exposed on the cell surface. Indeed, in contrast to the N-terminal anti-Aβ monoclonal antibody (6E10, 1:1,000; Signet Laboratories), which also binds full-length hAPP (Fig. S1*E*), the C-terminal Aβ40/42 antibody displayed no binding to cell-surface hAPP (Fig. S1*F*).

Anti-Aβ Immunotherapy Protects Against Loss of Visual Function and Retinal Damage. Initial support for the hypothesis that Aβ accumulation damages the eye was derived from studies testing the efficacy of anti-Aβ40 antibodies in preventing retinal damage in the *APOE4*-HFC model (42). Anti-Aβ40 administered at 3 mg/kg intraperitoneally weekly for 8 wk coincident with administration of HFC diet to 65-wk-old *APOE4* mice partially protected the animals from loss of visual function and RPE damage (42). Because the anti-Aβ40 therapy alone did not yield complete protection, two additional anti-Aβ antibodies, one targeting Aβ42 specifically and the other targeting both Aβ40 and Aβ42, were used here in the same experimental paradigm. To minimize the antibody constant region (Fc) effector function, these antibodies were either enzymatically deglycosylated (anti-Aβ42 or -Aβ40) (42) or mutated in the Fc region (anti-Aβ40/42) to eliminate binding to Fcγ receptors or complement C1q. Consequently, these antibodies were devoid of complement fixation activity or antibody-dependent cell-mediated cytotoxicity (44–48).

Visual function was monitored by analysis of b-wave electroretinograms (ERGs), a reliable measure of retinal activity and visual function (49). As we have previously shown (42, 50), the scotopic b-wave amplitudes in ERGs from affected *APOE4*-HFC mice are significantly reduced compared with controls. Remarkably, no attenuation in b-wave amplitude is detectable in the *APOE4*-HFC animals treated with anti-Aβ40/42 antibody; their ERGs are indistinguishable from age-matched, normal diet control *APOE*4 mice (Fig. 1*A*). The anti-Aβ40 antibody produces a lesser degree of protection similar to that observed in our previous study (42), whereas there is no statistically significant preservation of the b-wave amplitude in the anti-Aβ42–treated *APOE*4-HFC mice (Fig. S2*A*). Similar trends were observed in the a-wave amplitudes, reflecting the light responses of photoreceptors (Fig. S2*B*). To distinguish whether the reduction in b-wave amplitudes originated from impairment of photoreceptor activity or through impairment of bipolar cell function, we performed additional analysis of the ERGs. Comparison of b-wave and a-wave amplitude ratios at given flash intensities revealed that they are the same for control *APOE4*-ND and anti-Aβ40/42 antibody- and vehicle-treated *APOE4*-HFC animals over the range of applied flash intensities (Fig. S2*C*). This finding indicates that the attenuations in a- and b-wave amplitude are proportional and therefore, are attributable to light activity in photoreceptor cells (51). Analysis of the rod- vs. cone-driven components of the b-wave stimulus-response curves (51) shown in Fig. 1*A* shows that only rod-driven b-waves were attenuated in the affected *APOE4*-HFC mice, further localizing the visual function deficit to rod photoreceptors (Fig. S3).

Histological evaluation of sections of whole eyes through the optic nerve head revealed pathologic changes in the RPE and the presence of sub-RPE deposits in *APOE4*-HFC mice. RPE lesions are exemplified by vacuolization, pyknosis, hyper- and hypopigmentation, and infiltrating microglia. Morphologic analysis revealed that damage in the RPE is significantly less pronounced in the *APOE4*-HFC animals treated with the anti-Aβ40/42 antibody compared with any of the other *APOE4*-HFC groups (Fig. 1 *B–F*). Ultrastructural analysis of the RPE and Bruch's membrane confirmed Bruch's membrane thickening and sub-RPE deposit formation in the *APOE4*-HFC animals and the absence of these pathologic changes in the anti-Aβ40/42 antibody-treated *APOE4*-HFC and normal control *APOE4*-ND animals (Fig. 1 *G–I*).

We quantified RPE damage in *APOE4*-HFC mice by immunostaining RPE flat mounts with an antibody to the tight junction protein, zona occludens 1 (ZO-1), staining nuclei with Hoechst 33342, and analyzing the images for RPE size, integrity, and number using the Duke Ophthalmic Cell Analysis Program (DOCAP) that was developed by our group (Fig. 2). RPE cells were enlarged and frequently observed to be multinucleate in vehicle-treated *APOE4*-HFC mice compared with control *APOE4*-ND and anti-Aβ40/42 antibody-treated *APOE4*-HFC animals (Fig. 2 *A–C*). To quantify these changes in RPE cells, the area of each RPE cell in flat-mount images from all groups was plotted (Fig. 2*D*). The distribution of the normal RPE cell areas fell within two peaks that closely matched ($R^2 = 0.9961, AR^2 = 0.9959$) a double Gaussian model (Fig. 2*D*, dashed blue line) corresponding to two RPE cell populations, one consisting of smaller cells with a single nucleus and a second consisting of larger binucleate cells. Affected RPE cells with areas larger than that predicted by our theoretical model (Fig. 2*D*, red trace) were compared among experimental groups. Specifically, cell areas of 22,495 cells in 23 images of the central RPE from 17 mice were measured from the three groups (*APOE4*-ND, *APOE4*-HFC, and *APOE4*-HFC treated with 3 mg/kg anti-Aβ40/42). The threshold of large cells is shown in the graph (Fig. 2*D*). Based on this threshold, the area occupied by large cells in each group (as a percent of total area) was determined (summarized in Fig. 2*E*). Quantitative morphometric analysis revealed a statistically significant increase in the number of abnormally large RPE cells in the *APOE4*-HFC animals (mean large-cell area ratio percent of 16 ± 5% SD) compared with the control *APOE4*-ND (4 ± 2%). Strikingly, this abnormal RPE cell enlargement is greatly reduced in the anti-Aβ40/42–treated *APOE4*-HFC animals (6 ± 3%), almost to the number detected in the *APOE4*-ND control RPE cells (Fig. 2*E*). Comparisons of different regions of RPE flat mounts revealed that there is also a central to peripheral gradient of RPE damage in *APOE4*-HFC mice, where central RPE damage is more severe.

RPE flat mounts of human donor eyes were also analyzed. In contrast to mouse RPE cells, which are largely binucleate, previous studies have shown that only about 3% of human RPE cells are binucleate (52, 53). Examination of RPE flat mounts from human donor eyes with and without documented AMD revealed similar RPE abnormalities to those abnormalitites found in the affected *APOE4*-HFC mouse eyes. Examination of nine donor eyes, four with AMD (Table S1), revealed that, in the perimacular region of AMD eyes, multinucleate RPE cells were more common, and RPE cell area was consistently larger than in the donor eyes without history of ocular disease (Fig. 3), similar to changes seen by Al-Hussaini et al. (54).

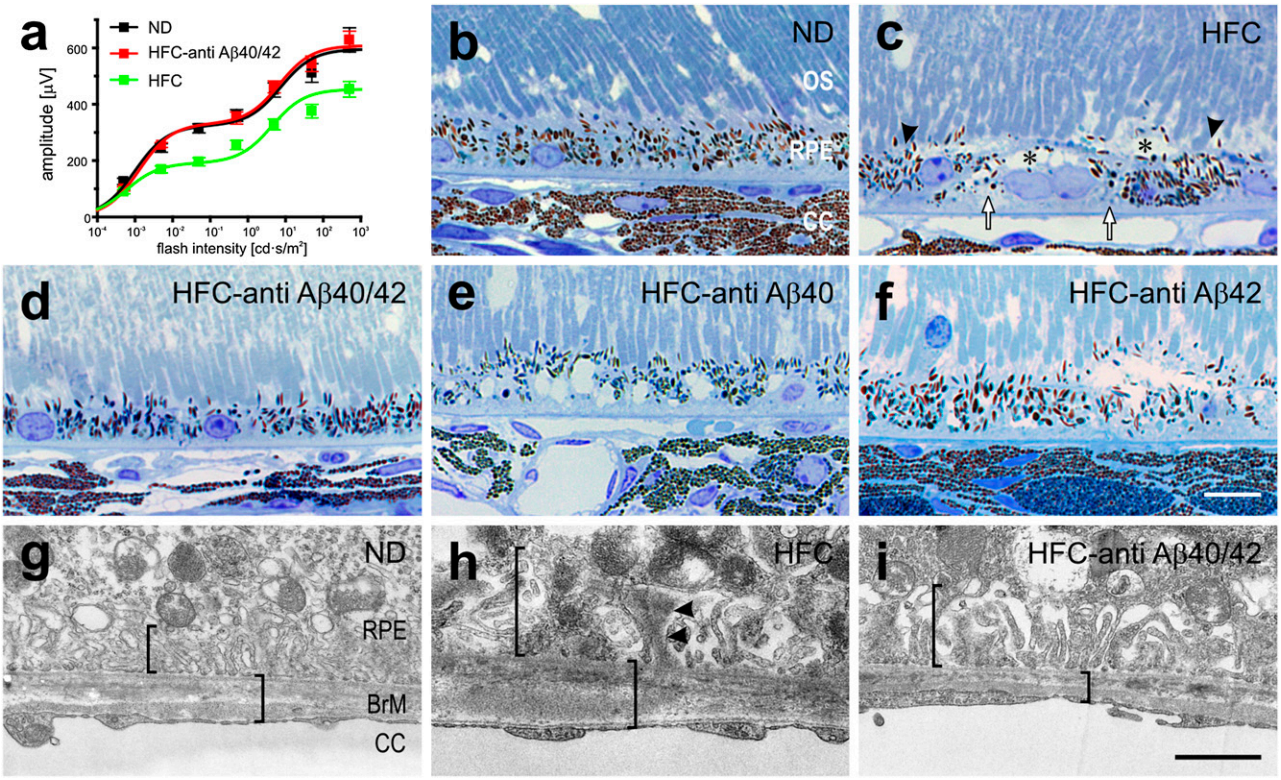

Fig. 1. Visual function and retinal pigmented epithelium (RPE) histology are protected in anti-Aβ40/42–treated *APOE4*-HFC mice. (*A*) Scotopic ERG flash responses. Stimulus response curves of b-wave amplitudes. Baseline ERGs obtained from normal *APOE4*-ND controls (black, ND) and affected *APOE4*-HFC vehicle-treated controls (green, HFC). b-Wave amplitudes are fully preserved in *APOE4*-HFC mice that received weekly 3 mg/kg i.p. anti-Aβ40/42 antibody injections (red, HFC-anti Aβ40/42), with no significant difference from *APOE4*-ND controls. Data are expressed as mean ± SEM. (*B–F*) Light microscopic images showing the outer segment/RPE/choroid interface in toluidine blue-stained sections from eyes of aged normal and HFC-fed *APOE4* mice after immunotherapy. The morphologies of the RPE in the normal *APOE4*-ND control mice (*B*) and *APOE4*-HFC mice injected with anti-Aβ40/42 (3 mg/kg; *D*) seem normal, whereas RPE in the vehicle- (*C*), anti-Aβ40– (*E*), and Aβ42- (*F*) treated *APOE4*-HFC mice exhibits damage, including large vacuoles (asterisks in *C*), hypo- and hyperpigmentation (arrowheads in *C*), and basal deposits and amorphous debris (arrows in *C*). (Scale bar: 10 μm.) (*G–I*) EMs of the interface between RPE and Bruch's membrane in *APOE4* mice. RPE basal infoldings (left bracket) and Bruch's membrane thickness (right bracket) appear normal in the anti-Aβ40/42–treated eye (*I*) compared with the normal *APOE4*-ND control mice (*G*). In contrast, in the HFC-fed *APOE4* mice (*H*), Bruch's membrane is thicker, and there are thick basal deposits with electron dense material among the basal infoldings (arrowheads in *H*). (Scale bar: 1 μm.) OS, outer segments; CC, choriocapillaris; BrM, Bruch's membrane.

Anti-Aβ Immunotherapy Reduces Ocular Aβ Deposits. We previously documented the presence of Aβ in sub-RPE deposits and choroidal neovascular lesions in *APOE4*-HFC mice (42, 43). ApoE, a major component of sub-RPE deposits and drusen in human eyes (55), is also a component of the basal deposits that form in the *APOE4*-HFC mice (56). In the current study, Aβ (rabbit anti-rodent Aβ, 39153; Signet) was again detected in apoE-containing (goat anti-human apoE; Calbiochem) basal deposits in the *APOE4*-HFC eyes, but it was notably absent from deposits in the anti-Aβ40/42–treated *APOE4*-HFC eyes (Fig. 4). This observation is consistent with the notion that Aβ is removed from sub-RPE deposits, leading to increased systemic levels as a consequence of the anti-Aβ40/42 therapy, which is detailed below.

Complement Deposition in *APOE4*-HFC Mice. Activated complement was detected in small patches associated with sub-RPE deposits in *APOE4* mice using a monoclonal antibody that detects C3 cleavage fragments: C3b/iC3b/C3c (clone 2/11 from HyCult Biotechnology) (57) (Fig. 5). Some C3 colocalizes within apoE-defined basal deposits (Fig. 5 *B* and *C*), whereas additional C3 immunoreactivity does not colocalize (Fig. 5*A*). A reduction in C3 fragment immunoreactivity is observed in anti-Aβ40/42–treated *APOE4*-HFC mice compared with untreated *APOE4*-HFC animals.

Activated complement was also quantified in plasma obtained from normal control *APOE4*-ND, affected *APOE4*-HFC, and anti-Aβ immunotherapy-treated *APOE4*-HFC animals using an ELISA for C3a/C3a desArg (Fig. 5*D*). HFC diet alone was associated with a statistically significant increase in complement activation, which was measured as elevated C3a plasma levels, although a wide range of plasma concentrations was detected. The plasma C3a levels in the immunotherapy-treated animals were not significantly different from those levels in the untreated *APOE4*-HFC group, suggesting that there is no systemic inhibition of the complement pathway by anti–Aβ40/42 therapy.

Plasma Aβ Concentrations Increase with Anti-Aβ Immunotherapy. One mechanism by which passive immunotherapy mediates amyloid clearance in Alzheimer's disease is thought to be through the net efflux of Aβ from the brain to the plasma, which is facilitated by systemic anti-Aβ antibodies acting as a peripheral sink and preventing additional amyloid deposition in the brain (58). Plasma Aβ levels increase in response to passive immunotherapy against Aβ in animal models of Alzheimer's disease (58–61). To determine if circulating Aβ levels increase as a consequence of anti-Aβ immunotherapy in the *APOE4*-HFC mice, plasma Aβ levels were measured and compared with plasma levels of circulating anti-Aβ antibodies. High comparable concentrations of all three anti-Aβ antibodies were achieved in the plasma of antibody-treated animals (Fig. S4*A*), and plasma levels of total Aβ (bound and unbound) were substantially elevated in mice treated with the anti-Aβ40 or anti-Aβ40/42 antibodies (Fig. S4*B*) but not in anti-Aβ42–treated animals. These results are consistent with the peripheral

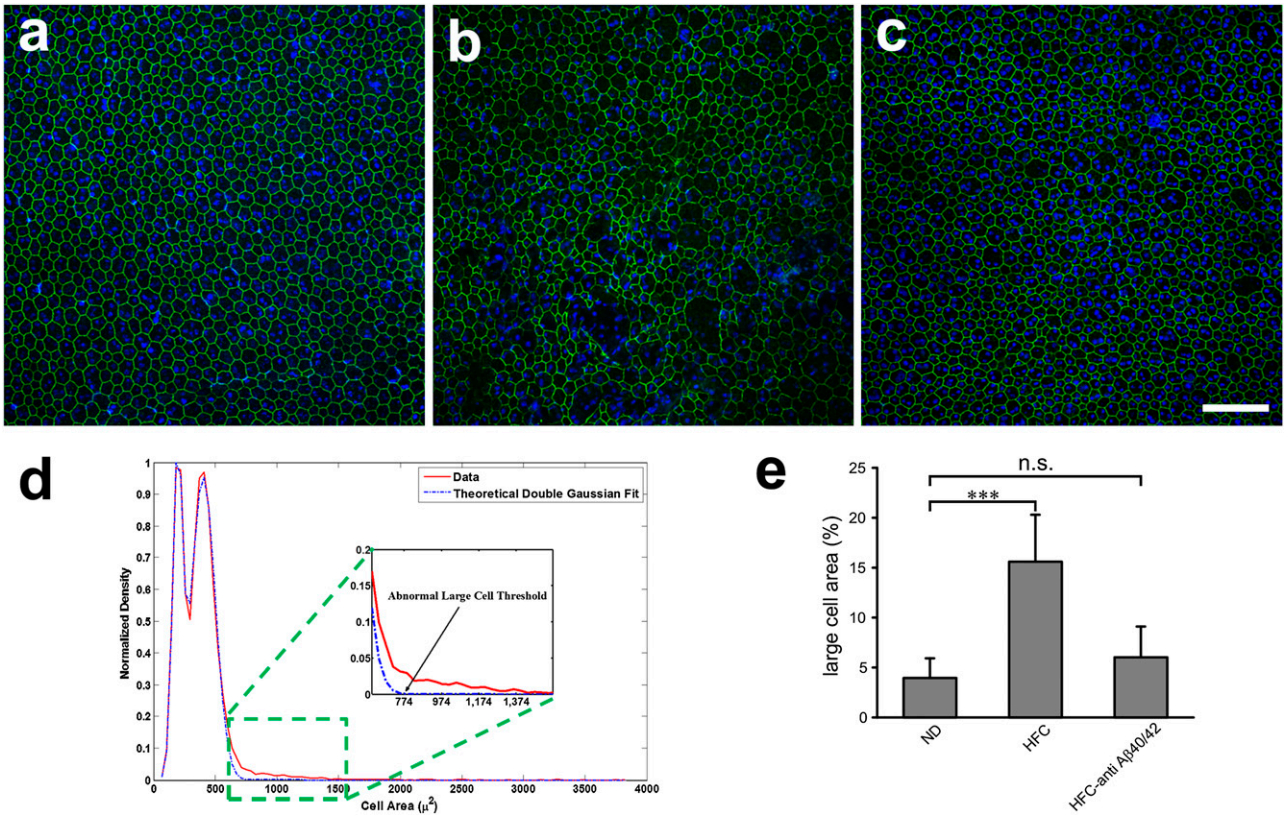

Fig. 2. Morphometric analysis of *APOE4* RPE flat mounts. (*A*–*C*) Confocal fluorescence images of flat mounts of the central RPE from (*A*) a normal 80-wk-old *APOE4*-ND mouse, (*B*) an age-matched affected *APOE4*-HFC mouse, and (*C*) an anti-Aβ40/42–treated *APOE4*-HFC mouse stained with Hoechst 33342 (blue) and anti–ZO-1 (green) and imaged RPE apical side up with the neural retina removed. (*A*) Anti–ZO-1 labeling of tight junctions reveals typical hexagonal shape of RPE cells, which are also largely binucleate in normal *APOE4*-ND mice. In *APOE4*-HFC mice (*B*), there are many more enlarged and multinucleate cells, whereas normal RPE morphology is largely maintained in the anti-Aβ40/42–treated APOE4-HFC mice (*C*). (Scale bar: 100 μm.) (*D*) Graph of cell area of 22,495 cells from 23 images of the central RPE from 17 mice in the three groups represented in *A*–C. The solid red line represents the normalized distribution of cell areas, which include areas of normal cells and abnormally large cells. Normal mouse RPE cells may have one or two nuclei. Positing that the normal cells with one nucleus and two nuclei would each have a normal distribution with a different mean and variance, the area distribution of the normal cells can be modeled by a double Gaussian curve. The dashed blue line represents the theoretical distribution of the normal cell area when this double Gaussian model was fitted to the data. Next, based on this model, the theoretical minimum size of the abnormally large cells was defined. The threshold of abnormally large cells was selected as the smallest area, with predicted distribution of less than 1 of 22,496 cells. (*E*) Morphometric analysis confirmed that there was a statistically significant increase in the percent of abnormally large RPE cells per unit area in vehicle-treated *APOE4*-HFC animals compared with normal *APOE4*-ND control mice (Student *t* test; ***$P < 0.00001$). In contrast, the percent of abnormally large cells in the anti-Aβ40/42–treated APOE4-HFC mice was reduced to near normal levels that were not statistically distinguishable from those levels of control *APOE4*-ND mice ($P = 0.1136$). Error bars represent SD (n.s., not significant).

sink hypothesis and provide a potential explanation of why the anti-Aβ42–treated animals were afforded little protection from Aβ-mediated RPE damage and vision loss.

Protection by Anti-Aβ40/42 Immunotherapy Is Dose-Dependent. We conducted a dose-response study on the bispecific anti-Aβ40/42 antibody in *APOE4*-HFC mice. Anti-Aβ40/42 was systemically administered weekly for 8 wk at 0-, 0.03-, 0.3-, and 3-mg/kg doses. ERGs confirmed a decrease in the b-wave amplitude in affected *APOE4*-HFC mice (0 mg/kg; vehicle injected) compared with the *APOE4*-ND controls (Fig. 6*A*). Like the findings already detailed, visual function was protected in *APOE4*-HFC mice that received the 3-mg/kg dosing of anti-Aβ40/42, but there was no statistically significant preservation of b-wave amplitudes at the 0.03- or 0.3-mg/kg dose levels (Fig. 6*A*). An antibody dose-dependent increase in plasma levels of Aβ (Fig. 6*B*) that corresponded to the plasma levels of the anti-Aβ40/42 antibody was again documented (Fig. 6*C*). Notably, the lower antibody doses were not sufficient to protect from visual function impairment, suggesting that there is a lower threshold of antibody concentration for effective protection. Interestingly, there was a small but statistically significant ($P = 0.039$) increase in the plasma Aβ levels of the HFC-fed group compared with the age-matched normal control group maintained on a normal diet (Fig. 6*B*, asterisk).

Discussion

Our current results show that antibody-based removal of Aβ from sub-RPE deposits in the *APOE4*-HFC model of AMD eliminates loss of visual function. A pathogenic role for Aβ in AMD was first proposed by Johnson et al. (39), who formulated the Aβ hypothesis of AMD. It was based in large part on the immunohistochemical colocalization of Aβ with activated complement components in sub-RPE deposits in human AMD donor eyes. Human RPE cells and retinal neurons express amyloid precursor protein (APP) and likely provide a local ocular source of amyloid peptides (39). Expression of APP, β-secretase, and neprilysin (a peptidase that degrades Aβ) and localization within the mouse RPE also have been shown (62). Moreover, in senescent neprilysin KO mice, Aβ accumulates in association with the RPE and Bruch's membrane, RPE vacuolization and damage is observed, and sub-RPE deposits are formed (62).

In the *APOE4*-HFC model of AMD, multiple factors that are known to modify AMD risk combine to manifest an AMD phenotype with striking concordance with human disease, exhibiting

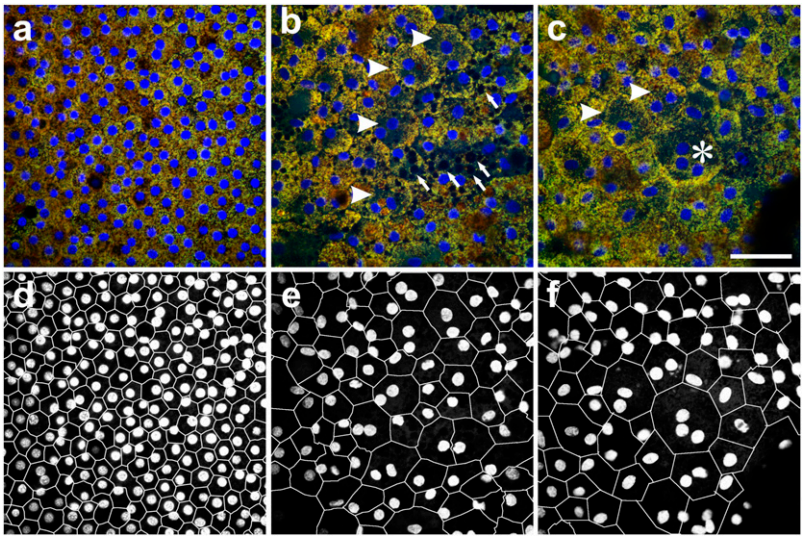

Fig. 3. Human RPE flat mounts. (*A–C*) Confocal fluorescence images of RPE flat mounts from equivalent perimacular regions (RPE basal side up). (*A*) Seventy-six year old (Y) Caucasian males with no history of ocular disease are shown; (*B* and *C*) 85 Y Caucasian females with clinically documented dry AMD in an area with multiple binucleate RPE cells (arrowheads in *B*) and vacuoles (arrows in *B*) and an area with a trinucleate RPE cell (asterisk in *C*) is shown. (*D–F*) *A–C* are segmented to highlight cell borders and nuclei using DOCAP. (Scale bar: 50 μm.)

age-dependent development of sub-RPE deposits and CNV (43, 63). Disease-associated changes observed include sub-RPE deposits that are immunopositive for Aβ, complement components and inflammatory markers (56), thickening of Bruch's membrane, patchy regions of RPE atrophy, and CNV. This phenotype presents in a temporal, incompletely penetrant, and noninvasive manner that is analogous to human AMD progression (43). Importantly, there is a robust, reproducible loss of visual function associated with the development of the AMD phenotype in these mice (42, 50) that mimics electrophysiological abnormalities that are observed in patients with AMD (64, 65). Although the exact mechanism by which *APOE4* targeted replacement and high-fat diet contributes to Aβ deposition in the sub-RPE region remains to be defined, conceivably, apoE4 genotype and HFC diet could together alter the local or systemic Aβ production or clearance. Consistent with this possibility, we found that plasma Aβ levels are significantly elevated in *APOE4*-HFC mice compared with normal diet controls (Fig. 6*B*).

In human AMD, Aβ deposition is associated with drusen in AMD eyes, where it accumulates and colocalizes with activated complement components (37, 39), but it is not typically observed in drusen from normal eyes (38). Aβ is a known activator of the complement system (37, 38, 66, 67) and has toxic effects on RPE cells (68). Oligomeric, protofibrillar, and mature fibrillar forms of Aβ have been detected in drusen using conformation-specific antibodies (40, 41) and classic amyloid stains like thioflavin T and Congo red (35, 37). Using the *APOE4*-HFC model, the current study also implicates Aβ in the pathogenesis and progression of AMD, providing evidence that it contributes to sub-RPE deposit formation, complement activation, RPE damage, and ultimately, retinal dysfunction. These studies suggest that Aβ acts as a trigger of the complement cascade either directly or as a secondary consequence of upstream damage that invokes inflammatory processes and RPE damage. Consistent with such a role is the remarkable protection from histopathologic changes and visual dysfunction afforded by anti-Aβ immunotherapy.

Immunotherapies targeting the Aβ peptide, using vaccines or antibodies, have been successfully applied to APP-based mouse models of Alzheimer's disease to reduce amyloid plaques and improve cognitive performance (69). Currently, in humans, there is no direct evidence that removing Aβ is harmful either in the brain or retina. However, there have been some complications associated with Alzheimer's disease clinical trials of Aβ-targeting therapies in which the observed side effects have been largely attributed to aseptic meningoencephalitis in response to active immunization with the first generation Aβ vaccine, AN-1792. This side effect was observed in 6% of patients in phase II clinical trials and eventually, was shown to be caused primarily by brain infiltration of T lymphocytes (70–72). The anti-Aβ antibodies used in this study were designed to target the C termini of Aβ peptides, because these epitopes are normally buried in the lipid bilayer in uncleaved APP and are predominantly exposed in the pathological state. These antibodies were also designed with a modified constant region (Fc) that does not bind to C1q or Fcγ receptors, and hence, they do not trigger complement activation or antibody-dependent cell-mediated cytotoxicity. The lack of antibody-induced complement activation of these Fc-modified anti-Aβ antibodies may be of high clinical relevance in the context of AMD treatment, because complement pathway dysfunction is strongly implicated in AMD pathogenesis (33–36). For example, the deglycosylated form of an anti-Aβ40 (2H6-D) retained efficacy in ameliorating Alzheimer's disease changes and behavioral deficits in Tg2576 mice, and it exhibited a significantly lower incidence of microhemorrhagic and inflammatory brain lesions than the parent antibody (47, 48). In human treatment with the humanized monoclonal anti-Aβ40 antibody, Ponezumab (PF-04360365), also without Fc effector function, thus far shows no incidence of pathologic side effects.* In contrast, in phase II Alzheimer's disease trials, treatment with the humanized monoclonal antibody, Bapineuzumab, which is directed against the N terminus of Aβ and does not have a modified Fc region, led to vasogenic edema in a significant subset of the Alzheimer's disease patients (73).

Initially, we showed that treatment with 2H6-D, the deglycosylated monoclonal antibody binding Aβ40, was associated with partial preservation of visual function and some attenuation of RPE damage in *APOE4*-HFC mice (42). The current study not

*Landen J, et al., Safety and pharmacokinetics following a single infusion of the anti-amyloid monoclonal antibody ponezumab (PF-04360365) in patients with mild-to-moderate Alzheimer's disease: Final results, Proceedings of the Alzheimer's Association International Conference on Alzheimer's Disease, July 14, 2010, abstr P4.

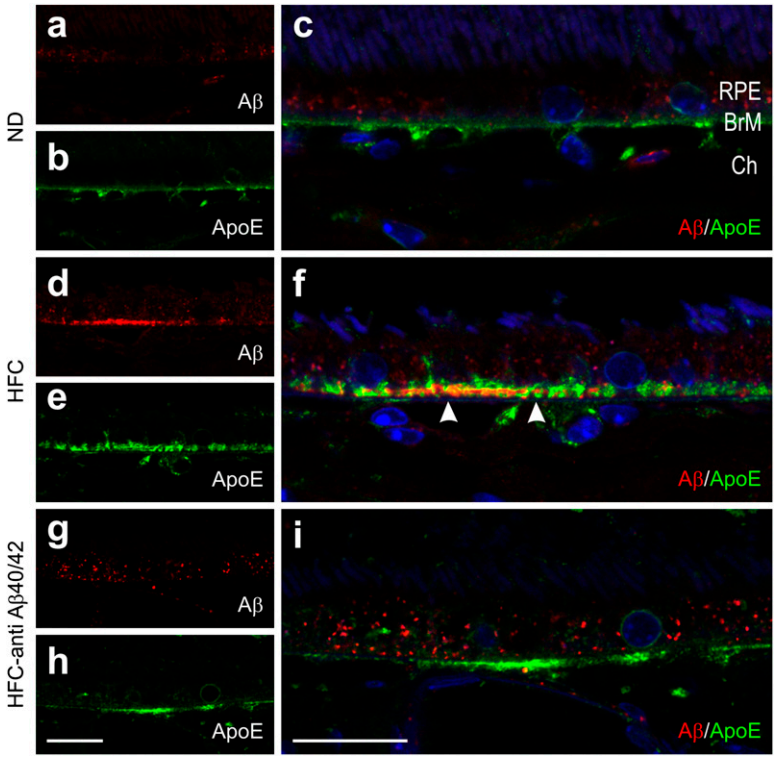

Fig. 4. Aβ levels are reduced in sub-RPE deposits of anti-Aβ40/42–treated *APOE4*-HFC mouse eyes compared with those eyes of vehicle-treated *APOE4*-HFC mice. Confocal immunofluorescence images depicting Aβ (red) and ApoE (green) detected in (*A–C*) normal diet *APOE4* mice (ND), (*D–F*) HFC-fed *APOE4* mice (HFC), and (*G–I*) immunotherapy-treated *APOE4*-HFC mice (HFC–anti-Aβ40/42). Aβ immunolocalizes within the choroid (Ch) and in ApoE-positive basal deposits (arrowheads in *F*). RPE autofluorescence (particulate red fluorescence) stemming from lipofuscin accumulation exhibited normal animal to animal variation. Cell nuclei are stained with Hoechst 33342 (blue). BrM, Bruch's membrane. (Scale bar: 20 μm.)

only confirmed these findings but also compared the efficacy of two anti-Aβ antibodies targeting different forms of Aβ. We show that systemic administration of an anti-Aβ40/42 bispecific antibody preserves retinal function and maintains normal RPE morphology. These findings support our hypothesis that decreasing ocular Aβ is sufficient to protect the RPE, and they suggest that amyloid-induced RPE damage leads to photoreceptor dysfunction and vision loss. The latter conclusion is based on the observed attenuation of scotopic ERGs without change in scotopic a- and b-wave ERG ratio and the lack of RPE damage in anti-Aβ40/42–treated *APOE4*-HFC mice.

Although little histological damage to photoreceptors was observed, visual function was affected, reflecting damage to cells in the neural retina. The attenuation in b-wave amplitudes that is observed in affected *APOE4*-HFC mice could be caused by changes in overall rod photoreceptor activity leading to reduced stimulation of rod bipolar cell light responses or changes at the rod to rod bipolar cell synaptic level. Analysis of the ratios of b- and a-wave amplitudes at given flash intensities revealed that they are the same for control *APOE4*-ND and anti-Aβ40/42 antibody- and vehicle-treated *APOE4*-HFC animals over the range of applied flash intensities. Therefore, attenuation in b-wave amplitude coincides with attenuation in a-wave amplitude without changing the b-/a-wave ratio. This finding supports the notion that changes in the photoreceptor activity, secondary to defects in RPE activity, are the likely mechanism for b-wave attenuation in HFC-fed *APOE4* animals rather than specific damage to rod bipolar cells (51). Moreover, analysis of the different photoreceptor components of the b-wave stimulus-response curves shows that rod-driven responses, but not cone-driven responses, are attenuated, further localizing the visual function deficit to rod photoreceptors (Fig. S3).

Rod-driven electrophysiological abnormalities are also observed in patients with AMD. Feigl et al. (64) showed that there is a functional impairment of the rods in early AMD patients seen on multifocal electroretinograms. Owsley et al. (65) showed that AMD patients had significant impairments in rod-mediated parameters of dark adaptation (including rod sensitivity) compared with age-matched adults with normal retinal health. These deficits were increasingly abnormal as disease severity increased, whereas cone-mediated parameters were not impaired in early AMD. These functional correlates in the *APOE4*-HFC mouse model of AMD also highlight the value of this disease model in the understanding of early-stage AMD pathogenesis.

Taken together, our results support the feasibility of immunotherapeutic strategies targeting Aβ as treatments for AMD. Because the presence of Aβ peptides in sub-RPE deposits has been implicated in the pathologic processes associated with AMD, we believe that treatment with anti-Aβ antibodies could produce improvements in retinal function deficits observed in both early and advanced stages of AMD, especially for those patients in whom Aβ deposition is a feature of their disease. The significance of the potential impact of an early-stage AMD therapy cannot be overstated considering that AMD is the leading cause of blindness in industrialized countries and that, currently, there are no effective therapies for the dry form of the disease, which affects the vast majority of AMD patients.

Materials and Methods

Mice. Mice were maintained in accordance with the Institutional Animal Care and Use Committee at Duke University. *APOE4*-targeted replacement mice expressing the E4 human apoE isoform were generated as described (74).

Human Tissue Procurement. Normal and AMD eyes used in these studies were obtained from the North Carolina Eye Bank, the Lions Eye Bank, and the

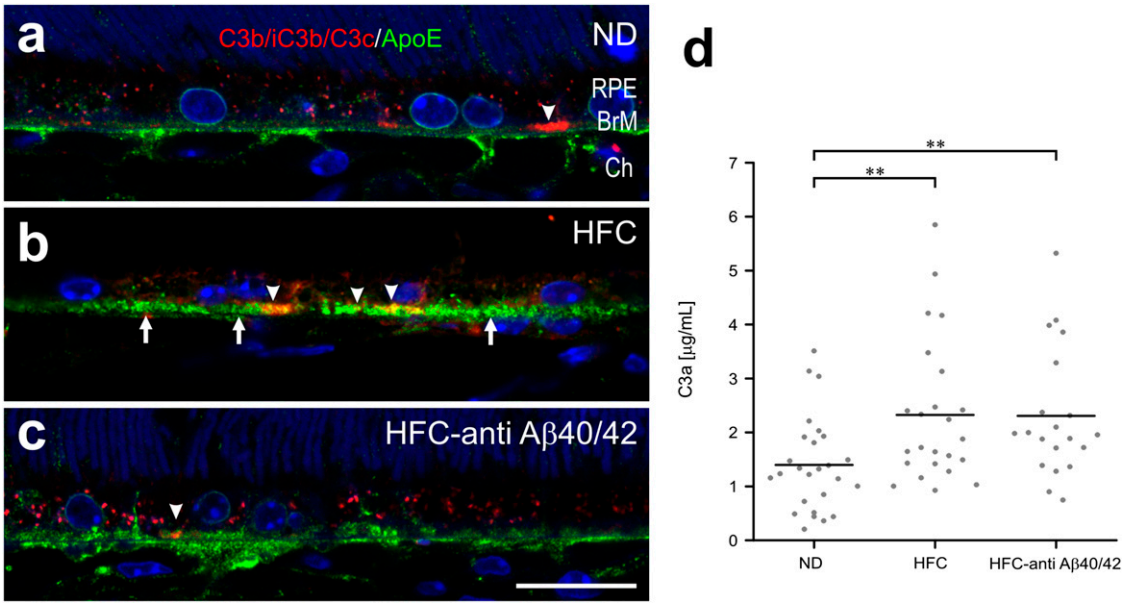

Fig. 5. Deposition of complement C3 fragments (C3b/iC3b/C3c) in *APOE4* mouse eyes and circulating in plasma. (*A*–*C*) Confocal immunofluorescence images depicting immunolocalization of C3b/iC3b/C3c- (red) and ApoE- (green) positive basal deposits (arrows in *B*) of 75-wk-old (*A*) normal control *APOE4*-ND (ND), (*B*) affected *APOE4*-HFC (HFC), and (*C*) anti-Aβ40/42–treated *APOE4*-HFC (HFC–anti-Aβ40/42) mice. C3 fragments are found in small, sub-RPE patches (arrowheads in *B*). These patches are diminished in anti-Aβ40/42–treated *APOE4*-HFC and normal control *APOE4*-ND mice compared with affected *APOE4*-HFC animals. BrM, Bruch's membrane; Ch, choroid; RPE, retinal pigment epithelium. (Scale bar: 20 μm.) (*D*) Levels of circulating C3a/C3a desArg were measured by ELISA in the plasma of normal control *APOE4*-ND (ND), affected *APOE4*-HFC (HFC), and anti-Aβ40/42–treated *APOE4*-HFC (HFC–anti-Aβ40/42) mice. There is a statistically significant increase in C3a plasma levels in both groups of the HFC-fed *APOE4* mice compared with the ND-fed controls (Student *t* test, $^{**}P < 0.01$). Black horizontal bars indicate average C3a levels in each group.

Medical Eye Bank of Florida within up to 9 h of death (with an average procurement time of 5 h and 29 min) (Table S1). Deidentified ophthalmic clinical records were obtained for donors with a history of AMD to confirm that they were from clinically diagnosed patients. A diagnosis of AMD was based on the clinical record and verified by gross examination of the posterior poles.

Antibodies. BALB/c female mice were immunized with keyhole limpet hemocyanin-conjugated Aβ28–40 or 29–42 peptides (Anaspec). Hybridomas were generated and screened by ELISA. Positive clones were expanded and IgG-purified using MabSelect protein A beads (Pierce).

Epitope Mapping. Ten-nanomolar biotinylated microscale peptide sets of 10 or 15 aa spanning the Aβ1–42 peptide (JPT Peptide Technologies GmbH) were bound to microtiter plates (NUNC Maxisorp) precoated with Streptavidin (Pierce) at 6 mg/mL in PBS, pH 7.4. Plates were washed and incubated with 5 μg/mL anti-Aβ40/42 (RN6G) for 1 h in PBS containing 0.5% BSA and 0.05% Tween 20. Detection used peroxidase-conjugated goat IgG against human κ-chain (MP Biomedicals) followed by TMB (3, 3′, 5, 5′ - Tetramethylbenzidine) substrate (KPL).

hAPP Transfection. The hAPP full-length coding sequence was amplified and cloned into the pcDNA3.2/V5/GW/D-TOPO vector (Invitrogen). The hAPP

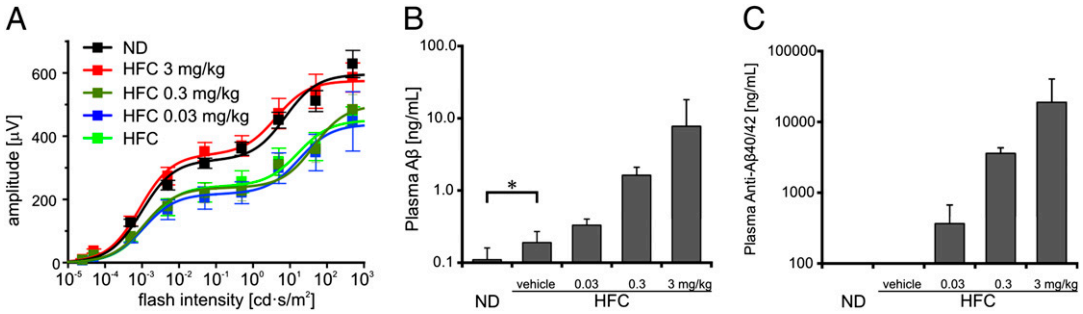

Fig. 6. Visual function is protected in anti-Aβ40/42–treated *APOE4*-HFC mice in a dose-dependent fashion that correlates with plasma levels of Aβ. (*A*) Dose-response study of ERG b-wave recovery in *APOE4*-HFC mice treated with three different doses of the anti-Aβ40/42 antibody. Baseline b-wave amplitudes are a function of flash intensity obtained from *APOE4*-ND controls (black, ND) and *APOE4*-HFC controls (green, HFC). As shown in Fig. 1*A*, b-wave amplitudes in the 3-mg/kg anti-Aβ40/42 antibody-treated *APOE4*-HFC animals (red, HFC 3 mg/kg) were fully preserved. In contrast, b-wave amplitudes in the 0.3- and 0.03-mg/kg anti-Aβ40/42 antibody-treated *APOE4*-HFC mice (olive green, HFC 0.3 mg/kg; blue, HFC 0.03 mg/kg, respectively) decreased to the same level as vehicle-treated *APOE4*-HFC animals (data are expressed as mean ± SEM). (*B* and *C*) Dose-dependent increase in plasma levels of Aβ and anti-Aβ40/42. Weekly i.p. injections of anti-Aβ40/42 at 0 (vehicle), 0.03, 0.3, and 3 mg/kg produced a statistically significant, dose-dependent increase in the plasma levels of total (bound and unbound) Aβ (*B*) that correlated with a dose-dependent increase in the concentrations of plasma anti-Aβ40/42 antibodies (*C*). Significant difference indicating a dose-dependent elevation of plasma (Aβ and anti-Aβ40/42) after increasing dose of antibody was shown by one-way ANOVA ($P < 0.0001$) and the posttest for linear trend (i.e., dose-dependent change), which was significant at $P < 0.0001$. In addition, there is a statistically significant increase in total Aβ plasma levels in response to the HFC diet compared with ND ($^{*}P < 0.05$; *B*). Error bars represent SD.

plasmid was transfected into transformed African green monkey kidney COS-7 cells with Fugene HD (Roche Diagnostics); 48 h later, cells were harvested for antibody staining and analyzed by FACS (Aria system; BD).

Diet and Immunotherapy. Aged male *APOE4* mice (n = 104; 65–87 wk) were maintained on a normal rodent chow diet [normal diet (ND), Isopurina 5001; Prolab], and a subset of these mice were switched to an HFC diet (n = 84; TD 88051; Harlan Teklad) for 8 wk. The *APOE4*-HFC mice were also subgrouped based on antibody treatment (Tables S2 and S3). Mice were randomly assigned to three treatment groups with even distribution by age.

Anti-Aβ antibody-injected animals received one time per week i.p. injections (3 mg/kg body weight/injection) of a deglycosylated (D) form of anti-Aβ40 (2H6-D, anti-Aβ33–40, mouse IgG2b; Pfizer) (48, 75), anti-Aβ42 (7G10-D, anti-Aβ28–42, mouse IgG1; Pfizer), or Fc-mutated anti-Aβ40/42 (RN6G, anti-Aβ25–42, human IgG2a; Pfizer), which recognizes the C termini of Aβ40 and Aβ42. Antibody doses and injection paradigms were based on established parameters (42).

ERG. ERGs were recorded using the Espion E^2 system (Diagnosys LLC) (42, 50). Data analysis and fitting were performed as described (51). Personnel responsible for ERGs and assessment of pathology were masked to the identity of treatment groups.

Histology. Mice were deeply anesthetized and perfused transcardially with saline followed by fixative (4% paraformaldehyde in phosphate buffer, pH 7.4, for immunohistochemistry or a mixture of 2% paraformaldehyde and 2% glutaraldehyde in phosphate buffer for semithin and ultra-thin sections). For semithin sections, eyeballs were enucleated; the cornea and lenses were removed, dehydrated, embedded in Epon–Spurr resin, cut at 500 nm, mounted on glass slides, and stained with toluidine blue. Sections were examined under a Zeiss Axioplan 2 microscope (Thornwood).

EM. Mouse eyes were embedded with a mixture of Epon and Spurr resins and polymerized at 60 °C for 36–48 h. Thin sections of ~80 nm were cut, mounted on copper grids, counterstained with uranyl acetate and Sato's lead, and examined on a Tecnai G2 TWIN transmission electron microscope (FEI).

Immunohistochemistry. Mouse posterior eyecups were embedded in agar and vibratome-sectioned at 50–100 μm. Sections were blocked in 10% normal donkey serum (Jackson Immunoresearch), incubated overnight with primary antibodies, incubated for 2 h in Alexa fluorophore-conjugated secondary antibody (Invitrogen), and counterstained with Hoechst 33342 (Invitrogen). Primary antibodies used were anti-rodent–specific Aβ (SIG-39157, 1:1,000; Covance), anti-human apoE (178479, 1:5,000; Calbiochem), and anti-mouse C3b/iC3b/C3c (HyCult clone 2/11, 1:1,000). Confocal images were acquired using a Leica SP5 laser-scanning confocal microscope.

RPE Flat-Mount Preparations. ***Mouse.*** The neural retina was dissected from unfixed posterior eyecups, leaving the RPE cell layer exposed, and then fixed overnight in methanol. RPE cells were stained with a rabbit antibody against ZO-1 (40–2200, 1:100; Invitrogen) and Hoechst 33342, and confocal images were captured on a Nikon Eclipse C1 microscope.
Human. RPE flat mounts (basal side up) were made from formalin-fixed human donor eyes with and without documented AMD; 4-mm-diameter punches just outside the macula (perimacular) were obtained, the retina and sclera were removed, and the punch was placed RPE side down on a slide. Choroid and Bruch's membrane were removed to expose the basal face of the RPE. The RPE was stained with Hoechst 33342, and images were collected using a Leica SP5 confocal microscope.

Morphometric analysis was performed with DOCAP software from images of RPE flat mounts. All images were corrected with respect to local changes in contrast, and after denoising, the image gradient, as a pilot estimate of the cell borders, was calculated. Erroneous borders were removed, and compensation was made for stippled nuclear Hoechst 33342 staining. Each closed contour was assumed to be an individual cell. Segmented images were reviewed by human graders, and errors in the automatic segmentation algorithm were manually corrected. Area, eccentricity, and other morphological properties were measured for each cell.

Aβ ELISA. Mesoscale discovery (MSD) standard 96-well plates were coated overnight at 4 °C with 2 μg/mL SIG-39153 (N-terminal mouse anti-Aβ capture antibody; Signet) diluted in PBS buffer. Biotinylated mouse monoclonal anti-Aβ antibody 4G8 (MSD) at 1 μg/mL was used for detection of mouse Aβ1-X with sulfo-tag streptavidin (MSD).

Antibody ELISA. Anti-Aβ40 and -Aβ40/42 were measured in mouse plasma by standard ELISA methods.

C3a ELISA. One hundred microliters 1 μg/mL rat anti-mouse C3a (also recognizes C3a desArg; BD Bioscience) were coated onto 96-well Nunc maxisorb plates, incubated overnight at 4 °C, and blocked with 1% BSA; then, dilutions of a C3a standard (BD Biosciences) and 1:300 dilutions of samples in 1% BSA were added for 2 h followed by sequential incubations with 1:500 dilution of biotinylated rat anti-mouse C3a, streptavidin-peroxidase (Sigma), and Sigma Fast OPD. OD at 450 nm was determined, and the concentration was calculated using a standard curve.

Statistical Analysis. RPE cell size data (Fig. 2*C*) and C3a plasma levels (Fig. 5*D*) were analyzed using an unpaired two-tailed Student t test. For data comparing the plasma antibody titer and total Aβ plasma level using the different doses of the same antibody, one-way ANOVA was applied (Fig. 6). For data comparing the plasma antibody titer and total Aβ plasma-level effect after the treatment of different classes of anti-Aβ antibodies, unpaired one-tailed Student t test was applied followed by Welch's correction (Fig. S4). Statistical tests for each experiment are described in the figure legends with relevant P values, and a significance level of 0.05 for all tests was used. Statistical analyses were performed in Excel, MATLAB, or GraphPad Prism statistical packages.

ACKNOWLEDGMENTS. We gratefully acknowledge support from generous benefactors of the University of California Santa Barbara Center for the Study of Macular Degeneration, Zhe Chen for generating the human APP plasmid, Likun (Sam) Xi for his help with the RPE cell segmentation, Mark Gilbert for assistance with FACS, and Danielle Pappas for helping with mouse serum ELISA. This work was supported by National Institutes of Health Grants R24 EY017404 (to L.V.J.), R01 EY019038 (to C.B.R.), and P30 EY005722 (to Duke Eye Center), the Research to Prevent Blindness, Inc. (RPB) Core Grants to the Duke Eye Center, the RPB Special Scholars Award (to C.B.R.), The Ruth and Milton Steinbach Fund (to C.B.R.), and the Macular Vision Research Foundation (to C.B.R.).

1. Jager RD, Mieler WF, Miller JW (2008) Age-related macular degeneration. *N Engl J Med* 358:2606–2617.
2. Klein R, Klein BE, Linton KL (1992) Prevalence of age-related maculopathy. The Beaver Dam Eye Study. *Ophthalmology* 99:933–943.
3. Vingerling JR, et al. (1995) The prevalence of age-related maculopathy in the Rotterdam Study. *Ophthalmology* 102:205–210.
4. Klein BE, Klein R, Lee KE (2002) Incidence of age-related cataract over a 10-year interval: The Beaver Dam Eye Study. *Ophthalmology* 109:2052–2057.
5. Penfold PL, Madigan MC, Gillies MC, Provis JM (2001) Immunological and aetiological aspects of macular degeneration. *Prog Retin Eye Res* 20:385–414.
6. Gehrs KM, Anderson DH, Johnson LV, Hageman GS (2006) Age-related macular degeneration—emerging pathogenetic and therapeutic concepts. *Ann Med* 38:450–471.
7. Gragoudas ES, et al. (2004) Pegaptanib for neovascular age-related macular degeneration. *N Engl J Med* 351:2805–2816.
8. Hooper CY, Guymer RH (2003) New treatments in age-related macular degeneration. *Clin Experiment Ophthalmol* 31:376–391.
9. Mordenti J, et al. (1999) Comparisons of the intraocular tissue distribution, pharmacokinetics, and safety of 125I-labeled full-length and Fab antibodies in rhesus monkeys following intravitreal administration. *Toxicol Pathol* 27:536–544.
10. Klein R, Klein BE, Jensen SC (1997) The relation of cardiovascular disease and its risk factors to the 5-year incidence of age-related maculopathy: The Beaver Dam Eye Study. *Ophthalmology* 104:1804–1812.
11. Mares-Perlman JA, et al. (1995) Dietary fat and age-related maculopathy. *Arch Ophthalmol* 113:743–748.
12. Seddon JM, Cote J, Rosner B (2003) Progression of age-related macular degeneration: Association with dietary fat, transunsaturated fat, nuts, and fish intake. *Arch Ophthalmol* 121:1728–1737.
13. Seddon JM, et al. (2001) Dietary fat and risk for advanced age-related macular degeneration. *Arch Ophthalmol* 119:1191–1199.
14. Vingerling JR, et al. (1995) Age-related macular degeneration is associated with atherosclerosis. The Rotterdam Study. *Am J Epidemiol* 142:404–409.
15. Edwards AO, et al. (2005) Complement factor H polymorphism and age-related macular degeneration. *Science* 308:421–424.
16. Hageman GS, et al. (2005) A common haplotype in the complement regulatory gene factor H (HF1/CFH) predisposes individuals to age-related macular degeneration. *Proc Natl Acad Sci USA* 102:7227–7232.
17. Haines JL, et al. (2005) Complement factor H variant increases the risk of age-related macular degeneration. *Science* 308:419–421.

18. Klein RJ, et al. (2005) Complement factor H polymorphism in age-related macular degeneration. *Science* 308:385–389.
19. Gold B, et al. (2006) Variation in factor B (BF) and complement component 2 (C2) genes is associated with age-related macular degeneration. *Nat Genet* 38:458–462.
20. Yates JR, et al. (2007) Complement C3 variant and the risk of age-related macular degeneration. *N Engl J Med* 357:553–561.
21. Baird PN, et al. (2006) Apolipoprotein (APOE) gene is associated with progression of age-related macular degeneration (AMD). *Hum Mutat* 27:337–342.
22. Fritsche LG, et al. (2009) Age-related macular degeneration and functional promoter and coding variants of the apolipoprotein E gene. *Hum Mutat* 30:1048–1053.
23. Haas P, et al. (2011) Genetic cardiovascular risk factors and age-related macular degeneration. *Acta Ophthalmol* 89:335–338.
24. Schmidt S, et al. (2002) A pooled case-control study of the apolipoprotein E (APOE) gene in age-related maculopathy. *Ophthalmic Genet* 23:209–223.
25. Zareparsi S, et al. (2004) Association of apolipoprotein E alleles with susceptibility to age-related macular degeneration in a large cohort from a single center. *Invest Ophthalmol Vis Sci* 45:1306–1310.
26. Zareparsi S, et al. (2005) Toll-like receptor 4 variant D299G is associated with susceptibility to age-related macular degeneration. *Hum Mol Genet* 14:1449–1455.
27. Kanda A, et al. (2007) A variant of mitochondrial protein LOC387715/ARMS2, not HTRA1, is strongly associated with age-related macular degeneration. *Proc Natl Acad Sci USA* 104:16227–16232.
28. Rivera A, et al. (2005) Hypothetical LOC387715 is a second major susceptibility gene for age-related macular degeneration, contributing independently of complement factor H to disease risk. *Hum Mol Genet* 14:3227–3236.
29. Dewan A, et al. (2006) HTRA1 promoter polymorphism in wet age-related macular degeneration. *Science* 314:989–992.
30. Yang Z, et al. (2006) A variant of the HTRA1 gene increases susceptibility to age-related macular degeneration. *Science* 314:992–993.
31. Allikmets R, The International ABCR Screening Consortium (2000) Further evidence for an association of ABCR alleles with age-related macular degeneration. *Am J Hum Genet* 67:487–491.
32. Stone EM, et al. (2004) Missense variations in the fibulin 5 gene and age-related macular degeneration. *N Engl J Med* 351:346–353.
33. Hageman GS, Mullins RF, Russell SR, Johnson LV, Anderson DH (1999) Vitronectin is a constituent of ocular drusen and the vitronectin gene is expressed in human retinal pigmented epithelial cells. *FASEB J* 13:477–484.
34. Johnson LV, Ozaki S, Staples MK, Erickson PA, Anderson DH (2000) A potential role for immune complex pathogenesis in drusen formation. *Exp Eye Res* 70:441–449.
35. Mullins RF, Russell SR, Anderson DH, Hageman GS (2000) Drusen associated with aging and age-related macular degeneration contain proteins common to extracellular deposits associated with atherosclerosis, elastosis, amyloidosis, and dense deposit disease. *FASEB J* 14:835–846.
36. Sakaguchi H, et al. (2002) Clusterin is present in drusen in age-related macular degeneration. *Exp Eye Res* 74:547–549.
37. Anderson DH, et al. (2004) Characterization of beta amyloid assemblies in drusen: The deposits associated with aging and age-related macular degeneration. *Exp Eye Res* 78:243–256.
38. Dentchev T, Milam AH, Lee VM, Trojanowski JQ, Dunaief JL (2003) Amyloid-beta is found in drusen from some age-related macular degeneration retinas, but not in drusen from normal retinas. *Mol Vis* 9:184–190.
39. Johnson LV, et al. (2002) The Alzheimer's A beta-peptide is deposited at sites of complement activation in pathologic deposits associated with aging and age-related macular degeneration. *Proc Natl Acad Sci USA* 99:11830–11835.
40. Luibl V, et al. (2006) Drusen deposits associated with aging and age-related macular degeneration contain nonfibrillar amyloid oligomers. *J Clin Invest* 116:378–385.
41. Isas JM, et al. (2010) Soluble and mature amyloid fibrils in drusen deposits. *Invest Ophthalmol Vis Sci* 51:1304–1310.
42. Ding JD, et al. (2008) Targeting age-related macular degeneration with Alzheimer's disease based immunotherapies: Anti-amyloid-beta antibody attenuates pathologies in an age-related macular degeneration mouse model. *Vision Res* 48:339–345.
43. Malek G, et al. (2005) Apolipoprotein E allele-dependent pathogenesis: A model for age-related retinal degeneration. *Proc Natl Acad Sci USA* 102:11900–11905.
44. Armour KL, Atherton A, Williamson LM, Clark MR (2002) The contrasting IgG-binding interactions of human and herpes simplex virus Fc receptors. *Biochem Soc Trans* 30: 495–500.
45. Armour KL, Clark MR, Hadley AG, Williamson LM (1999) Recombinant human IgG molecules lacking Fcgamma receptor I binding and monocyte triggering activities. *Eur J Immunol* 29:2613–2624.
46. Armour KL, van de Winkel JG, Williamson LM, Clark MR (2003) Differential binding to human FcgammaRIIa and FcgammaRIIb receptors by human IgG wildtype and mutant antibodies. *Mol Immunol* 40:585–593.
47. Carty NC, et al. (2006) Intracranial administration of deglycosylated C-terminal-specific anti-Abeta antibody efficiently clears amyloid plaques without activating microglia in amyloid-depositing transgenic mice. *J Neuroinflammation* 3:11.
48. Wilcock DM, et al. (2006) Deglycosylated anti-amyloid-beta antibodies eliminate cognitive deficits and reduce parenchymal amyloid with minimal vascular consequences in aged amyloid precursor protein transgenic mice. *J Neurosci* 26: 5340–5346.
49. Niemeyer G (1998) Selective rod- and cone-ERG responses in retinal degenerations. *Digit J Ophthalmol* 4(10).
50. Malek G, Jamison JA, Mace B, Sullivan P, Bowes Rickman C (2008) ERG responses and microarray analysis of gene expression in a multifactorial murine model of age-related retinal degeneration. *Adv Exp Med Biol* 613:165–170.
51. Herrmann R, et al. (2010) Phosducin regulates transmission at the photoreceptor-to-ON-bipolar cell synapse. *J Neurosci* 30:3239–3253.
52. Friedman E, Ts'o MO (1968) The retinal pigment epithelium. II. Histologic changes associated with age. *Arch Ophthalmol* 79:315–320.
53. Ts'o MO, Friedman E (1967) The retinal pigment epithelium. I. Comparative histology. *Arch Ophthalmol* 78:641–649.
54. Al-Hussaini H, Schneiders M, Lundh P, Jeffery G (2009) Drusen are associated with local and distant disruptions to human retinal pigment epithelium cells. *Exp Eye Res* 88:610–612.
55. Anderson DH, et al. (2001) Local cellular sources of apolipoprotein E in the human retina and retinal pigmented epithelium: Implications for the process of drusen formation. *Am J Ophthalmol* 131:767–781.
56. Swaroop A, Chew EY, Bowes Rickman C, Abecasis GR (2009) Unraveling a multifactorial late-onset disease: From genetic susceptibility to disease mechanisms for age-related macular degeneration. *Annu Rev Genomics Hum Genet* 10:19–43.
57. Mastellos D, et al. (2004) Novel monoclonal antibodies against mouse C3 interfering with complement activation: Description of fine specificity and applications to various immunoassays. *Mol Immunol* 40:1213–1221.
58. DeMattos RB, et al. (2001) Peripheral anti-A beta antibody alters CNS and plasma A beta clearance and decreases brain A beta burden in a mouse model of Alzheimer's disease. *Proc Natl Acad Sci USA* 98:8850–8855.
59. DeMattos RB, Bales KR, Cummins DJ, Paul SM, Holtzman DM (2002) Brain to plasma amyloid-beta efflux: A measure of brain amyloid burden in a mouse model of Alzheimer's disease. *Science* 295:2264–2267.
60. Lemere CA, et al. (2003) Evidence for peripheral clearance of cerebral Abeta protein following chronic, active Abeta immunization in PSAPP mice. *Neurobiol Dis* 14:10–18.
61. Vasilevko V, Xu F, Previti ML, Van Nostrand WE, Cribbs DH (2007) Experimental investigation of antibody-mediated clearance mechanisms of amyloid-beta in CNS of Tg-SwDI transgenic mice. *J Neurosci* 27:13376–13383.
62. Yoshida T, et al. (2005) The potential role of amyloid beta in the pathogenesis of age-related macular degeneration. *J Clin Invest* 115:2793–2800.
63. Malek G, et al. (2006) Initial observations of key features of age-related macular degeneration in APOE targeted replacement mice. *Adv Exp Med Biol* 572:109–117.
64. Feigl B, Brown B, Lovie-Kitchin J, Swann P (2005) Cone- and rod-mediated multifocal electroretinogram in early age-related maculopathy. *Eye (Lond)* 19:431–441.
65. Owsley C, McGwin G, Jr., Jackson GR, Kallies K, Clark M (2007) Cone- and rod-mediated dark adaptation impairment in age-related maculopathy. *Ophthalmology* 114:1728–1735.
66. Kurji KH, et al. (2010) Microarray analysis identifies changes in inflammatory gene expression in response to amyloid-beta stimulation of cultured human retinal pigment epithelial cells. *Invest Ophthalmol Vis Sci* 51:1151–1163.
67. Wang J, et al. (2009) Amyloid-beta up-regulates complement factor B in retinal pigment epithelial cells through cytokines released from recruited macrophages/microglia: Another mechanism of complement activation in age-related macular degeneration. *J Cell Physiol* 220:119–128.
68. Bruban J, et al. (2009) Amyloid-beta(1-42) alters structure and function of retinal pigmented epithelial cells. *Aging Cell* 8:162–177.
69. Hardy J, Selkoe DJ (2002) The amyloid hypothesis of Alzheimer's disease: Progress and problems on the road to therapeutics. *Science* 297:353–356.
70. Ferrer I, Boada Rovira M, Sánchez Guerra ML, Rey MJ, Costa-Jussá F (2004) Neuropathology and pathogenesis of encephalitis following amyloid-beta immunization in Alzheimer's disease. *Brain Pathol* 14:11–20.
71. Nicoll JA, et al. (2003) Neuropathology of human Alzheimer disease after immunization with amyloid-beta peptide: A case report. *Nat Med* 9:448–452.
72. Orgogozo JM, et al. (2003) Subacute meningoencephalitis in a subset of patients with AD after Abeta42 immunization. *Neurology* 61:46–54.
73. Prins ND, Visser PJ, Scheltens P (2010) Can novel therapeutics halt the amyloid cascade? *Alzheimers Res Ther* 2:5.
74. Sullivan PM, et al. (1997) Targeted replacement of the mouse apolipoprotein E gene with the common human APOE3 allele enhances diet-induced hypercholesterolemia and atherosclerosis. *J Biol Chem* 272:17972–17980.
75. Wilcock DM, et al. (2004) Passive amyloid immunotherapy clears amyloid and transiently activates microglia in a transgenic mouse model of amyloid deposition. *J Neurosci* 24:6144–6151.